ISBN: 978-3-95450-214-1 ISSN: 2673-5490 doi:10.18429/JACoW-IPAC2021-TUPAB111

# LAYOUT OF THE LASER HEATER FOR FLASH2020+

Ch. Gerth*, E. Allaria, A. Choudhuri, L. Schaper, E. Schneidmiller, S. Schreiber, M. Tischer, P. Vagin, M. Vogt, L. Winkelmann, M.V. Yurkov, J. Zemella
Deutsches Elektronen-Synchrotron DESY, Hamburg, Germany

*Abstract*

The major upgrade FLASH2020+ of the FEL user facility FLASH includes an improved injector layout for the generation of the high-brightness electron beam as well as an externally seeded FEL beamline. Microbunching gain of initial modulations or shot-noise fluctuations degrade the electron beam quality, which is in particular harmful to the external seed process. To minimise the microbunching gain by a controlled increase of the uncorrelated energy spread, the installation of a laser heater is foreseen directly upstream of the first bunch compression chicane. In this paper, we present the layout of the laser heater section, which follows the original proposal published almost 20 years ago and differs in several aspects from the common layout implemented at many other FEL facilities. The considerations that have been made for the optimisation of the laser heater parameters are described in detail.

## INTRODUCTION

High-gain, single-pass free-electron lasers (FELs) [1–6] require high-brightness electron bunches with kiloampere peak currents, which are typically compressed in several stages by off-crest acceleration in combination with magnetic dipole chicanes. Random longitudinal charge density modulations occurring at the electron gun can be amplified by collective effects during bunch compression [7] or longitudinal space charge effects [8]. This process is referred to as microbunching instability [9, 10] and potentially degrades the FEL performance and is in particular detrimental to external seeding schemes [3, 11].

A laser heater (LH) was proposed in [8] for the mitigation of microbunching instability at the FLASH facility. An optical laser is superimposed on the electron beam in a short undulator, and the induced energy modulation due to the resonant laser-electron interaction is transformed in a dispersive section into an uncorrelated energy spread which is large enough to damp the microbunching gain but small enough to not degrade the FEL performance. The layout for a LH for the Linac Coherent Light Source (LCLS) [2] was reported in [12] and its successful realisation demonstrated in [13]. A similar layout was then implemented at FERMI [14], PAL-XFEL [15] and European XFEL [16].

The FLASH2020+ upgrade project [17] of the FLASH user facility [18] foresees the implementation of external seeding in the XUV and soft X-ray region [19]. Beam dynamic simulations predict that an induced energy spread in the range 10–20 keV is required for an effective suppression of the microbunching instability.

* christopher.gerth@desy.de

## GENERAL LAYOUT

Installation of the LH system is foreseen in the injector downstream of the first accelerating module and 3rd-harmonic linearisers. The conceptual layout of the LH section, as depicted in Fig. 1, follows the original proposal by Saldin *et al.* [8] and differs in some aspects from the common layout [13–16] where the LH undulator is located in the dispersive straight section of a 4-dipole chicane.

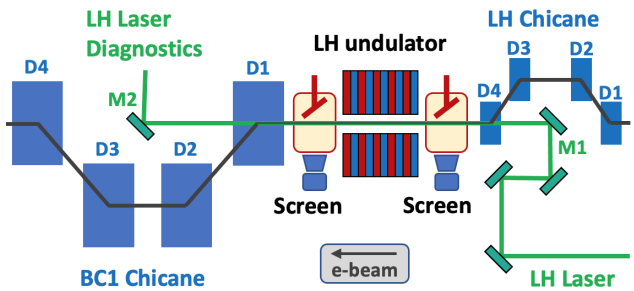


Figure 1: Schematic layout of the LH section at FLASH. Electron beam direction from left to right. Not to scale.

At FLASH, the correlated energy distribution due to off-crest acceleration would lead to beam tilts in the dispersive section of such a chicane, and, therefore, the LH undulator is located in the straight section of the electron beamline. For the in-coupling of the LH laser, an in-vacuum mirror (denoted M1 in Fig. 1) is used to deflect the LH laser by 90 degrees onto the nominal electron beam axis and a 4-dipole LH chicane to guide the electron beam around the in-vacuum mirror M1.

Furthermore, the LH laser system will provide laser pulses at a comparatively short wavelength of 532 nm, which allows efficient heating and longitudinal smearing of the imprinted energy modulation in the subsequent bunch compression chicane BC1 with a nominal longitudinal dispersion $R_{56}$ = 140 mm. This will drastically reduce the formation of any remaining density modulations due to the energy modulation induced by the LH and, therewith, effects such as trickle heating [13].

Two screen stations equipped with Chromox scintillation screens will enable simultaneous measurement of the LH laser and electron beam to achieve spatial overlap of both beams in the LH undulator.

## LH ELECTRON BEAMLINE SECTION

The superconducting accelerator of FLASH is operated with up to 800 µs-long radio-frequency (RF) pulses at 10 Hz repetition rate which can be filled with a flexible electron bunch pattern with a maximum repetition of 1.0 MHz to

ISBN: 978-3-95450-214-1 ISSN: 2673-5490 doi:10.18429/JACoW-IPAC2021-TUPAB111



serve two FEL beamlines [20]. At the location of the LH after the 3rd-harmonic lineariser, the nominal electron beam energy is 146 MeV with a maximum correlated energy spread of 3% (peak-peak) for bunch compression. The nominal longitudinal dispersion $R_{56}$ of the first bunch compression chicane BC1 directly after the LH amounts to 140 mm. Table 1 summarises the electron beam parameters.

Table 1: Electron Beam Parameters

| Parameter | Unit | Value |
|---|---|---|
| Electron beam energy, $E_b$ | MeV | 146 |
| Max. correlated energy spread (p-p) | % | 3.0 |
| Electron beam size (rms), $\sigma_{x,y}$ | µm | 250 |
| Bunch train repetition rate | Hz | 10.0 |
| Bunch train length | µs | 800 |
| Intra-train repetition rate | MHz | 1.0 |
| BC1 chicane $R_{56}$ | mm | 140 |

## LH LASER SYSTEM

In order to match the electron bunch train pattern (see Table 1), bursts of up to 800 laser pulses with an intra-burst repetition rate of 1.0 MHz are required at a rate of 10 Hz. These bursts of laser pulses will be generated at a center wavelength of 1 064 nm using a hybrid Yb:fiber / Nd:YVO4 laser system. The bandwidth-limited output pulses with a length of 11 ps (FWHM) will be frequency-doubled to 532 nm by a 2nd-harmonic process in a Lithium Tri-Borate (LBO) crystal. The linear-polarised laser pulses in the green will have a peak power of up to 2.0 MW in the burst and are transported from the laser laboratory by a 1:1 imaging telescopic beamline with a length of about 50 m to the LH electron beamline. Optical elements will then be used to tailor the transverse spot size (see Table 2) and position for the overlap with the electron beam.

Table 2: LH Laser Parameters

| Parameter | Unit | Value |
|---|---|---|
| Wavelength, $\lambda_L$ | nm | 532 |
| Peak power, $P_L$ | MW | 2.0 |
| Spot size (rms), $\sigma_L$ | µm | 100 - 1000 |

## LH UNDULATOR

The LH undulator is of planar type with vertical field direction to match the linear polarisation of the LH laser. To establish the LH process for a fixed LH laser wavelength $\lambda_L$ and given electron beam energy $E_b$, the LH undulator needs to fulfil the resonance condition for the fundamental wavelength:

$$\lambda_L \equiv \frac{\lambda_u}{2\gamma^2}\left(1+\frac{K^2}{2}\right), \quad (1)$$

with $\gamma = E_b/mc^2$, and the undulator $K$ value and undulator period $\lambda_u$. The $K$ value depends on the magnet material, undulator period and gap. Several aspects need to be considered for an optimisation of these two undulator parameters.

At the location of the LH undulator, there is an increased probability of radiation losses originating from dark current from the electron gun or field emission from the 3rd-harmonic accelerating module during the up to 800 µs-long RF accelerating pulses (see Table 1). Therefore, SmCo has been chosen as magnet material for its increased radiation hardness, although the remanence is about 10% lower compared to commonly used NdFeB magnet structures. Furthermore to avoid beam losses, the minimum gap of the LH undulator needs to be optimised to avoid a drastic reduction of the beam stay clear for the vacuum chamber compared to the 34 mm of the standard beam pipe diameter.

Figure 2 depicts the relation between undulator period and $K$ value for various undulator gaps as solid lines. The $K$ value decreases for a certain period length when the gap is increased. The resonance condition of the undulator is shown for the nominal and maximum electron beam energy as a blue and red dotted line, respectively. A target value of $K \approx 1.4$ was chosen to achieve an efficient interaction of the LH laser and electron beam in the LH undulator. The dotted blue line, representing the nominal beam energy $E_b$ = 146 MeV, reaches $K = 1.4$ at a period length $\lambda_u$ just below 44.0 mm. A period length of $\lambda_u$ = 43.0 mm was chosen as this enabled to fit $N = 11$ full periods into the maximum available total length for the LH undulator. To allow operation at the maximum beam energy of $E_b$ = 150 MeV with some safety margin, a minimum gap of 22.0 mm was chosen. The LH undulator parameters are summarised in Table 3.

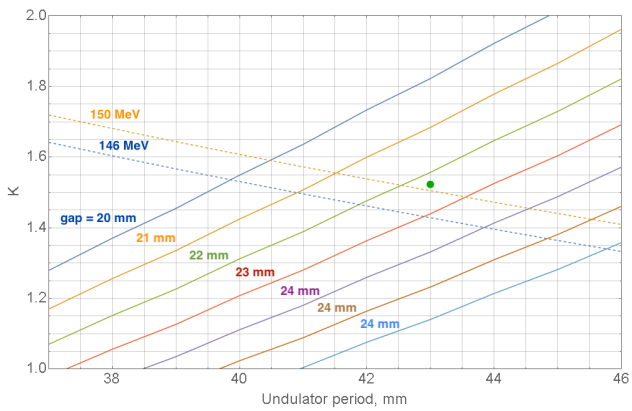


Figure 2: Optimisation of LH undulators parameters. For more details see text.

Table 3: LH Undulator Parameters

| Parameter | Unit | Value |
|---|---|---|
| Magnet material | | $Sm_2Co_{17}$ |
| Period length, $\lambda_u$ | mm | 43.0 |
| Number of full periods, $N$ | | 11 |
| Nominal $K$ value | | 1.43 |
| Minimum gap | mm | 22.0 |

ISBN: 978-3-95450-214-1 ISSN: 2673-5490 doi:10.18429/JACoW-IPAC2021-TUPAB111

Figure 3 presents the LH undulator $K$ value and corresponding gap setting calculated for the electron beam energy range 130–150 MeV for injector operation. The $K$ values range from 1.1 to 1.5 and the corresponding gap settings from 26 mm to 22 mm, respectively. The values of $K = 1.43$ and gap setting of 22.5 mm for the nominal beam energy of 146 MeV are indicated.

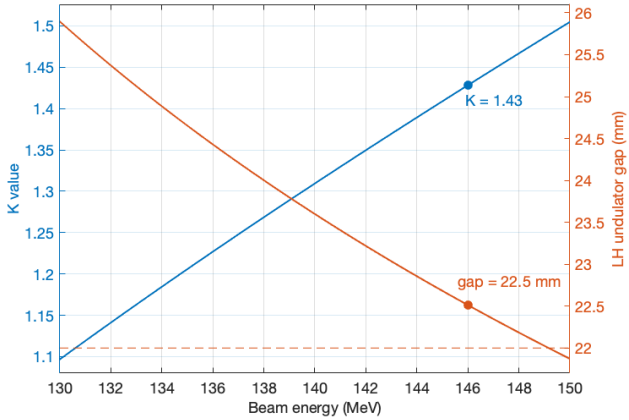


Figure 3: LH undulator K value (left) and gap (right) for the resonance wavelength of 532 nm and electron beam energy range 130–150 MeV. The values for the nominal beam energy of 146 MeV are indicated.

## INDUCED ENERGY SPREAD

Assuming that the electron and LH laser beam transverse sizes do not change much in the LH undulator, the induced rms energy spread by the laser-electron interaction can be approximated analytically by [13]:

$$\sigma_E = \frac{K \cdot JJ(K) \cdot N \cdot \lambda_u}{\gamma / mc^2} \sqrt{\frac{\sigma_L^2}{2(\sigma_x^2 + \sigma_L^2)}} \frac{1}{\sigma_L} \sqrt{\frac{P_L}{P_0}}, \quad (2)$$

where $P_L$ is the peak laser power, $P_0 = 8.7$ GW, JJ(K) the usual Bessel function factor for a planar undulator, and $\sigma_x$ and $\sigma_L$ the rms electron and laser beam sizes, respectively. The induced energy spread has been calculated for the pararmeters given in Tables 1-3, and the result is shown for various rms laser spot sizes in Fig. 4. As can be seen, a desired induced energy spread in the order 10–20 keV can be reached, however, without much overhead compared to other facilities due to power limitations of the high-repetition rate, frequency-doubled laser beam. For $\sigma_L = 250$ µm, the LH laser spot size is matched to the rms electron beam size.

## SUMMARY

LH systems have proven to be important components of single-pass high-gain FELs for the suppression of longitudinal microbunching instability by inducing a controllable slice energy spread. Within the FLASH2020+ Upgrade project, a LH will be integrated between the 3rd-harmonic accelerating module and the first bunch compression chicane

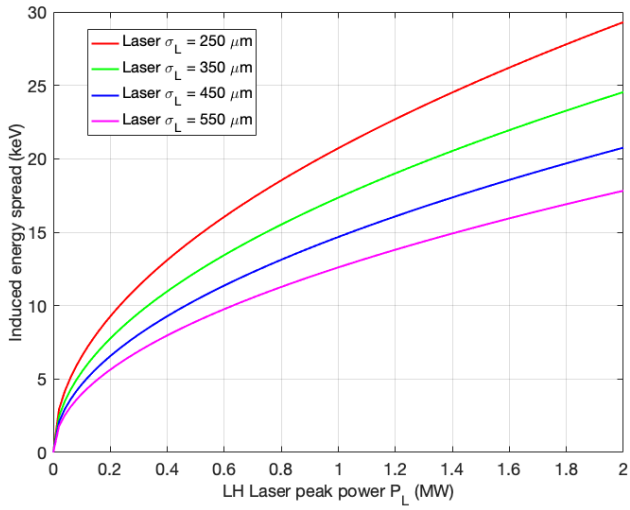


Figure 4: Induced energy spread for various rms LH laser spot sizes. For $\sigma_L = 250$ µm the LH laser spot size is matched to the rms electron beam size.

BC1. A screenshot of the 3D model showing the LH accelerator section is depicted in Fig. 5. The layout of the LH follows the original proposal with a LH undulator located in a dispersion-free, straight electron beam section and a subsequent chicane for the conversion of the induced energy modulation into an uncorrelated energy spread. The relatively short LH laser wavelength of 532 nm in combination with a large $R_{56}$ of BC1 will lead to an efficient heating with reduced probability of effects such as trickle heating [13]. To minimise the risk of radiation damage for the LH undulator magnets due to the high duty cycle of the accelerator, SmCo has been chosen as magnet material for its radiation hardness. The LH undulator has been optimised within the given space constraints for a $K$ value of about 1.4 and a large gap to reduce radiation losses.

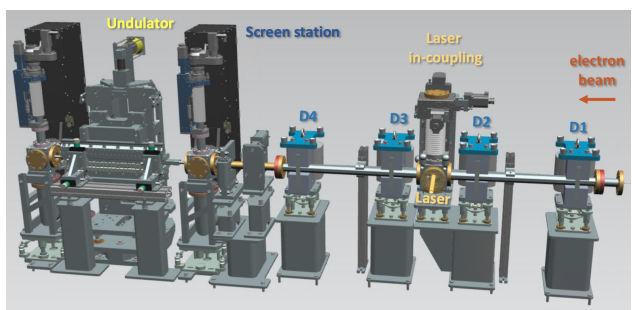


Figure 5: Screenshot of 3D model of the LH section including the LH chicane, LH undulator, and two screen stations up- and downstream of the LH undulator.

## ACKNOWLEDGEMENTS

The authors would like to thank all members of the FLASH2020+ project team that have contributed to the design study and engineering layout of the LH system.

ISBN: 978-3-95450-214-1 ISSN: 2673-5490 doi:10.18429/JACoW-IPAC2021-TUPAB111



## REFERENCES


[1] W. Ackermann *et al.*, "Operation of a free-electron laser from the extreme ultraviolet to the water window", *Nat. Photonics*, vol. 1, pp. 336–342, 2007. doi:10.1038/nphoton.2007.76

[2] P. Emma *et al.*, "First lasing and operation of an ångstromwavelength free-electron laser", *Nat. Photonics*, vol. 4, no. 9, pp. 641–647, 2010. doi:10.1038/nphoton.2010.176

[3] E. Allaria *et al.*, "Highly coherent and stable pulses from the fermi seeded free-electron laser in the extreme ultraviolet", *Nat. Photonics*, vol. 6, no. 10, pp. 699–704, 2012. doi:10.1038/nphoton.2012.233

[4] H.-S. Kang *et al.*, "Hard x-ray free-electron laser with femtosecond-scale timing jitter", *Nat. Photonics*, vol. 11, no. 11, pp. 708–713, 2017. doi:10.1038/s41566-017-0029-8

[5] W. Decking *et al.*, "A MHz-repetition-rate hard X-ray free-electron laser driven by a superconducting linear accelerator", *Nat. Photonics*, vol. 14, no. 6, pp. 391–397, 2020. doi:10.1038/s41566-020-0607-z

[6] E. Prat *et al.*, "A compact and cost-effective hard x-ray free-electron laser driven by a high-brightness and low-energy electron beam", *Nat. Photonics*, vol. 14, no. 12, pp. 748– 754, 2020. doi:10.1038/s41566-020-00712-8

[7] E. L. Saldin, E. A. Schneidmiller, and M. V. Yurkov, "Klystron instability of a relativistic electron beam in a bunch compressor", *Nucl. Instrum. Methods Phys. Res., Sect. A*, vol. 490, pp. 1–8, 2002. doi:10.1016/S0168-9002(02)00905-1

[8] E. L. Saldin, E. A. Schneidmiller, and M. V. Yurkov, "Longitudinal space charge-driven microbunching instability in the tesla test facility linac", *Nucl. Instrum. Methods Phys. Res., Sect. A*, vol. 528, no. 1, pp. 355–359, 2004. doi:10.1016/j.nima.2004.04.067

[9] D. Ratner *et al.*, "Time-resolved imaging of the microbunching instability and energy spread at the linac coherent light source", *Phys. Rev. ST Accel. Beams*, vol. 18, p. 030704, Mar. 2015. doi:10.1103/PhysRevSTAB.18.030704

[10] S. Di Mitri and S. Spampinati, "Microbunching instability study in a linac-driven free electron laser spreader beam line", *Phys. Rev. Accel. Beams*, vol. 20, p. 120701, Dec. 2017. doi:10.1103/PhysRevAccelBeams.20.120701

[11] P. Rebernik Ribič *et al.*, "Coherent soft x-ray pulses from an echo-enabled harmonic generation free-electron laser", *Nat. Photonics*, vol. 13, no. 8, pp. 555–561, 2019. doi:10.1038/s41566-019-0427-1

[12] Z. Huang *et al.*, "Suppression of microbunching instability in the linac coherent light source", *Phys. Rev. ST Accel. Beams*, vol. 7, p. 074401, Jul. 2004. doi:10.1103/PhysRevSTAB.7.074401

[13] Z. Huang *et al.*, "Measurements of the linac coherent light source laser heater and its impact on the x-ray free-electron laser performance", *Phys. Rev. ST Accel. Beams*, vol. 13, p. 020703, Feb. 2010. doi:10.1103/PhysRevSTAB.13.020703

[14] S. Spampinati *et al.*, "Laser heater commissioning at an externally seeded free-electron laser", *Phys. Rev. ST Accel. Beams*, vol. 17, p. 120705, Dec. 2014. doi:10.1103/PhysRevSTAB.17.120705

[15] L. JaeHyun *et al.*, "PAL-XFEL laser heater commissioning", *Nucl. Instrum. Methods Phys. Res., Sect. A*, vol. 843, pp. 39–45, 2017. doi:10.1016/j.nima.2016.11.001

[16] M. Hamberg *et al.*, "Electron beam heating with the European XFEL laser heater", in *Proc. FEL'17*, Santa Fe, NM, USA, 2017, paper WEP018, pp. 458–459.

[17] E. Allaria *et al.*, "FLASH2020+ plans for a new coherent source at DESY", presented at IPAC'21, Campinas, Brazil, May 2021, paper TUPAB086, this conference.

[18] K. Tiedtke *et al.*, "The soft x-ray free-electron laser FLASH at DESY: Beamlines, diagnostics and end-stations", *New J. Phys.*, vol. 11, p. 023029, 2009. doi:10.1088/1367-2630/11/2/023029

[19] L. Schaper *et al.*, "XUV and soft x-ray external seeding at flash: Activities and future plans", presented at IPAC'21, Campinas, Brazil, May 2021, paper THPAB115, this conference.

[20] B. Faatz *et al.*, "Simultaneous operation of two soft x-ray freeelectron lasers driven by one linear accelerator", *New J. Phys.*, vol. 18, no. 6, p. 062002, Jun. 2016. doi:10.1088/1367-2630/18/6/062002